RSC Advances

ROYAL SOCIETY OF CHEMISTRY

www.rsc.org/advances

Cite this: DOI: 10.1039/c0xx00000x

www.rsc.org/xxxxxx

ARTICLE TYPE

Curly Graphene Nanosheets Modified by Nanoneedle-like Manganese Oxide for Electrochemical Capacitors

Xiaoqing Yu[a,b], Kaiqi Li[a,b], Haihui Zhou*[a,b], Shudan Wei [a,b],ChangjunZhang[a,b], XueyingLi[a,b] and YafeiKuang*[a,b]

a State Key Laboratory for Chemo/Biosensing and Chemometrics, Hunan University, Changsha, China; Fax: +86-731-88713642; Tel:+86-731-88821603; E-mail: yafeik@163.com

b College of Chemistry and Chemical Engineering, Hunan University, Changsha, China; Fax: +86-731-88713642; Tel:+86-731-88821603; E-mail: yafeik@163.com

A modified Hummers method and an aqueous solution synthesis method have been adopted to prepare curly graphene nanosheets/manganese oxide (CGN/MnO_2) composite using multiwalled carbon nanotubes and $KMnO_4$ as precursorsin this paper. The morphologies and structure have been characterized by a range of microscopes and other techniques. MnO_2 acicular crystals with about 5 nm in diameter and about 100 nm in length crisscross were uniformly dispersed on the surface of CGN to form three-dimensional nanostructured CGN/MnO_2 composite. The electrochemical results show that the CGN/MnO_2 composite electrode delivered a specific capacitance of 224 F g^{-1} at the current density of 1 A g^{-1} in 1 M Na_2SO_4 solution, which was about 2.7 times higher than that of pure CGN (83 F g^{-1}). Meanwhile, CGN/MnO_2 composite exhibits high current charge-discharge capability and long-time cycling stability (the capacitance remains 95% of the initial value after 10,000 cycles). The excellent electrochemical capacitance performance of CGN/MnO_2 composite was explained as follows: (1) As 10 wt% nanoneedle-like MnO_2 is attached uniformly on the surface of CGN, the electronic conductivity of CGN/MnO_2 composite is improved. Meanwhile, the modification of CGN by a small quantity of nanoneedle-like MnO_2 further increases the interlayer distance of CGN, and the diffusivity of ions between composite electrode materials is improved as well. (2) Three-dimensional nanostructured CGN/MnO_2 composite can make the full use of the double layer capacitance of CGN and the pseudocapacitive performance of MnO_2.

1. Induction

Composite electrode materials for supercapacitors have been widely studied and aregenerally classified into three types: composite of different carbon-based materials[1], composite of carbon-based materials and pseudocapacitive electrode materials[2, 3], and composite of different psuedocapacitive electrode materials[4-6]. Ke-Ning Sun et al prepared three-dimensional (3D) nanostructured graphene nanosheets (GN)-carbon nanotubes (CNTs) hybrids as appealing supercapacitor (SC) electrode materials with a high specific capacitance of 413 F g^{-1}, which was higher than that of GN or CNTs.[7] Zhang et al synthesized quasi graphene nanosheets (QGN)/RuO_2 composite combining the advantages of the pseudocapacitance of RuO_2 with that of the stable double-layer capacitance of QGN.[8] Wang et al prepared polypyrrole/poly(3,4-ethylenedioxythiophene) (PPy /PEDOT), and its potential window was up to 1 V in 1 M $LiClO_4$ solution, which waslarger than 0.4 V for PPy.[9]Wang and Zhang loaded various amounts ofRuO_2·xH_2O on TiO_2 nanotubes to obtain a maximum specific capacitance of 1263 F g^{-1}.[10] Research on composite electrode materials is to develop the advantages of different materials in electrochemical capacitive performance and overcome their deficiencies. So, after a large amount of studies on the electrochemical capacitive composite materials, researchers have noticed that it's extremely important to find the best percentage of the constituent materials, and the optimal electrochemical capacitive performance can be obtained only with the best ratio of each component.

Carbon-based nano-materials, with excellent thermal, electrical and mechanical properties, and high surface area, have received considerable attention[11, 12]. Among the carbon-based materials, carbon nanotubes (CNTs) have captured a lot of attentions of many researchers. CNTs possess superior properties such as electrical conductivity[13-15], thermal property[16-18] and mechanical strength[19-21], which can promote their application as supercapacitor electrode materials. CNTs are hollow nanostructures consisting of carbon atoms, which look like cylindrical tubes rolled up by graphene sheets. However, typical CNTs within the micrometre range are easily aggregated into entangled ropes or masses and both ends of CNTs are closed, which prevent ion transport both in the inner and on the surface of CNTs, and reduce specific surface area of CNTs[22, 23], especially for multi-walled carbon nanotubes (MWCNTs), the capacitance is difficult to be fully explored. Hence, the low capacitive performance of CNTs hinders their application in electronic double layer capacitor (EDLC)[24]. As a result, modification of CNTs is required to realize better properties. Transverse cutting and longitudinal unzipping of CNTs to form curved graphene can be an effective method to improve the specific surface area and open the ends[25-27]. The obtained structure of the product is similar to graphene nanosheets but is not flat. Hence, the modified CNTs with large surface area

including the outer and inner walls can be termed as curly graphene nanosheets (CGN). Although the increase in surface area of CGN can result in larger double layer capacitance, the whole capacitance of CGN is still not satisfied. Therefore it is necessary to combine CGN with other electrode materials with high capacitance.

Transition metal oxides such as RuO_2[28], NiO[29], MnO_2[30] and Co_3O_4[31] are excellent electrode materials for pseudocapacitors. As an excellent pseudocapacitive electrode material, RuO_2 has good conductivity, high specific capacitance (as high as 1300 F g^{-1})[32], wide potential window, and high cycling stability[33-35]. However, as a precious transition metal oxide, the high cost of RuO_2 becomes a hurdle for its wide applications. Instead, some inexpensive pseudocapacitive materials have attracted the attentions of researchers. Among them, MnO_2 has been widely applied in electrochemical capacitors for its low cost, abundance and environmentally friendly nature[36], and the theoretical specific capacitance of MnO_2 is up to 1370 F g^{-1}.[37] However, the poor electronic conductivity (10^{-5}-10^{-6} S cm^{-1})[38] and the attenuation of the electrochemical properties during the adopt process of MnO_2 restricted its application in SCs.[36]An effective way to improve the supercapacitive performance is to combine metal oxides with carbon-based materials, which can not only contribute to electrical double layer capacitance but also support MnO_2 to avoid restacking. E.Raymundo-Piñero et al made use of CNTs as an alternative additive replacing carbon black to improve the electrical conductivity of MnO_2 electrode to build capacitors, proved that the specific capacitance values referred to the oxide (α-MnO_2•nH_2O) increasedwhen increasing the amount of CNTs, and pointed out that the active mass ofα-MnO_2 was more accessible to a large enough amount of CNTs.[39] Sang-Bok Ma et al clearly stated that when a small amount of MnO_2 was dispersed uniformly over porous carbonaceous materials, the high specific capacitance was delivered.[40]Graphene oxide-MnO_2 nanocomposites were also reported as supercapacitor electrode materials, and showed a specific capacitance of 111.1 F g^{-1} at 1 A g^{-1} in 1 M Na_2SO_4, and 84% of the initial capacitance retained after 1000 cycles.[41] Although the combination of metal oxides with carbon-based materials has shown its supercapacitor performance enhancement, the electrochemical performance is still not satisfied and needs further improvements.

To the best of our knowledge, there is still no study reporting the supercapacitor application of combination of CGN and MnO_2. Herein, we report a simple synthesis of CGN modified by MnO_2 as supercapacitor electrode materials. The CGN synthesized from CNTs with a unique structure not only has a high surface area, but also support the MnO_2 more uniformly. The obtained CGN/MnO_2 composite showed that MnO_2 with nanoneedle-like structure wascrisscrossed uniformly on the surface of CGN, which effectively reduced the agglomeration of CGN, increased the specific surface area (from 104 m^2 g^{-1} to 138 m^2 g^{-1}), and kept the good conductivity. Then the CGN/MnO_2 composite was investigated as supercapacitor electrode in an aqueous electrolyte in both three-electrode and two-electrode configurations.

2. Experimental section

2.1. Chemicals and materials

All reagents (Sinopharm Chemical Reagent Co., Ltd., China) were of analytical grade. Ultrapure water was used in the work. The multi-walled carbon nanotubes (MWCNTs, purity >97%) with 5-15 μm in length and 60-100 nm in diameter were commercially supplied (L-MWNT-60100, Shenzhen Nanotech Port Co., Ltd.).

2.2. Synthesis of unzipped MWCNTs

Unzipped MWCNTs were synthesized by modified Hummers method. 1 g of MWCNTs and 0.5 g of sodium nitrate were dissolved in 46 mL of concentrated sulfuric acid (98%) in a 250 mL flask at first. Then the mixture was stirred in an ice bath at a temperature below 10°Cfor 1 h. 5 g of potassium permanganate was added to the suspension under vigorous stirring. After removal of the ice bath, the mixture was stirred at 35 °C for 4 h. Then, 100 mL of ultrapure water was slowly added with vigorous agitation, and the diluted suspension was stirred for another 30 min. After the suspensionwas cooled down to room temperature, 5 mL of H_2O_2 (30 wt%) and 180 mL of water were added to the mixture. The mixture was washed and centrifuged with 10 vol% HCl, ethanol and ultrapure water for several times. The resultant unzipped MWCNTs suspension was washed until the pH was close to 7 and dried at 60 °C under vacuum for 24 h.

2.3. Preparation of curly graphene nanosheets (CGN)

CGN was prepared by a hydrothermal method. 150 mg of the as-prepared unzipped MWCNTs were dispersed in 75 mL of ultrapure water accompanying ultrasonic treatment for 1 h. Then, the solution was transferred into a 100 mL of Teflon-lined stainless autoclave. Subsequently, the autoclave was sealed and heated at 180 °C for 2 h. The as-prepared sample was washed with ethanol and ultrapure water for several times, and vacuum-dried at 60 °C for 12 h to obtain CGN.

2.4. Synthesis of CGN/MnO_2 composites

To synthesize CGN/MnO_2 composite, 45 mg CGN was dispersed in 25 mL of water, followed by ultrasonic treatment for 1 h. Subsequently, the suspension was treated by sonifer cell disrupter for 0.5 h. Then 8 mL aqueous ammonia and 18.16 mg $KMnO_4$ were

added into the mixture and heated to 100 °C for 2 h. After the solution was cooled down to room temperature, the ultimate suspension was filtered and washed with ultrapure water for several times. Finally, the sample was dried under a vacuum oven at 60 °C for 12 h.

2.5. Morphology and structure characterization

The morphologies of the obtained samples were characterized by scanning electron microscope (SEM) (Hitachi S-4800, Japan) and transmission electron microscope (TEM). Raman spectra were measured on a Raman spectrometer (Labram-010, France) using 632 nm laser excitation. The nitrogen adsorption-desorption isotherms and the pore size distribution curves were measured by the nitrogen physical sorption (Beckman Coulter SA-3100, USA).

2.6. Electrochemical measurements

Cyclic voltammetry (CV) and galvanostatic charge-discharge measurements were performed in a three-electrode system on a CHI 660E electrochemical workstation (Shanghai Chenhua Instrument, China), using saturated calomel electrode (SCE) as the reference electrode and platinum gauze electrode as the counter electrode. The working electrode was prepared by dropping 1 mg mL^{-1} of suspension (10 μL) onto a glassy carbon electrode (3.0 mm diameter) and dried at room temperature for 12 h.The electrical conductivity was measured by SZT-2 four-probe conductivity meter (Suzhou Tongchuang Electronics Ltd., China).

3. Results and discussion

3.1. Morphology and Structure

Figure 1 illustrates the preparation process of CGN/MnO_2 composite. Modified Hummers method and a simple reduction process were selected to prepare the CGN, and the as-prepared CGN was well dispersed in ultrapure water and reacted with the added $KMnO_4$ at 100 °C for the deposition of MnO_2 on the surface of CGN. The process was expressed by the reaction below:

$$C+2KMnO_4 \rightarrow K_2MnO_4+MnO_2+CO_2\uparrow$$

Although the CGN was reduced via hydrothermal method, some oxygen containing functional groups were still existed on the surface of it. Predictably, $KMnO_4$ reacted preferentially with carbon atoms containing oxygen groups, therefore a small quantity of the generated MnO_2 nanoneedles grew and preferentially clung to the surface of CGN to improve the physicochemical properties of the CGN/MnO_2 composite.

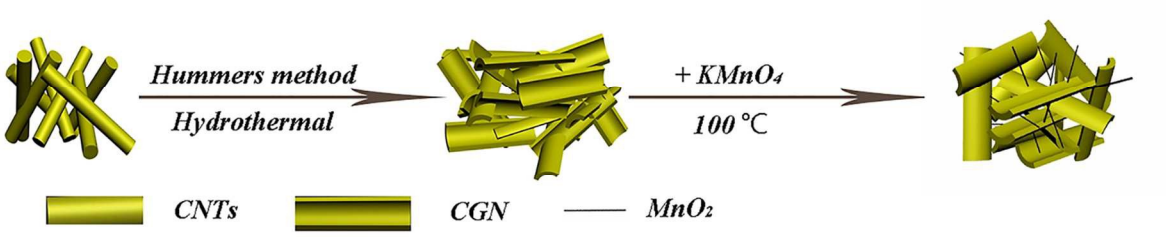

Figure 1 Schematic illustration of the synthesis of CGN/MnO_2.

The SEM and TEM images of the as-prepared CGN and CGN/MnO_2 composite are shown in Figure 2a-2d. The MWCNTs were split into the CGN shown in Figure 2a displaying curly graphene nanosheetsafter the modified Hummers and the hydrothermal treatments. Figure 2b shows that a large number of MnO_2 nanoneedles were attached uniformly on the surface of CGN to form 3D structural CGN/MnO_2 nanocomposite. TEM image in Figure 2c shows that nanoneedle-like manganese dioxide with ~5 nm in diameter and ~100 nm in length grown firmly on the inner and outer walls of CGN, which greatly improved the electronic conductivity of the CGN/MnO_2. Figure 2d shows masses of CGN lamellas were mixed with a large amount of MnO_2 nanoneedles to form a good ion diffusion channel.

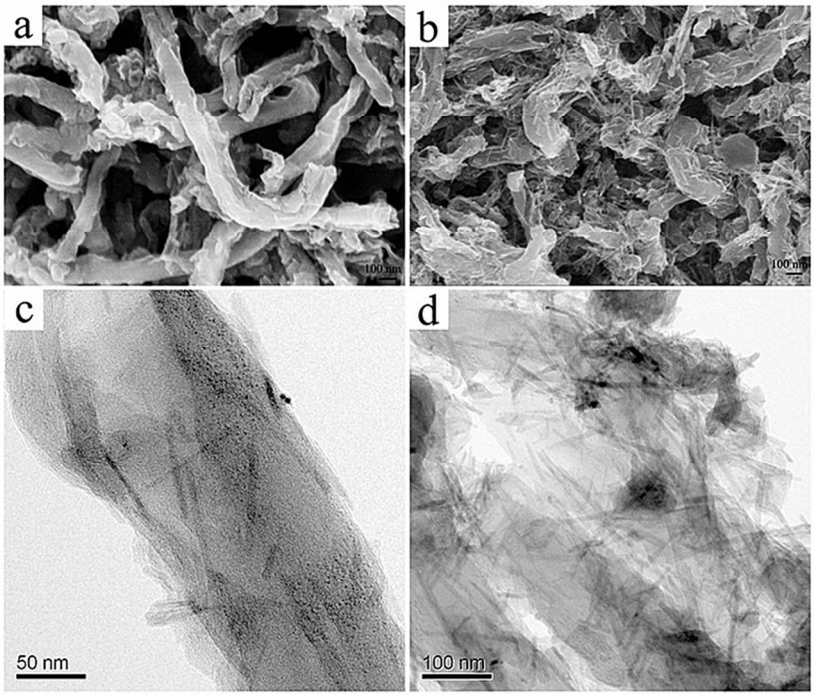

Figure 2 SEM images of CGN (a) and CGN/MnO_2 (b), TEM images of CGN/MnO_2 (c) and (d).

The XRD patterns of MWCNTs, unzipped MWCNTs, CGN and CGN/MnO_2 are shown in Figure 3. The XRD pattern of MWCNTs showed a sharp peak at 26.3° with the interlayer spacing of 3.4 Å. After the oxidation, a peak at 2θ=10.3° appeared, corresponding to the interlayer spacing of about 8.5 Å, confirming the formation of the oxygen-containing function groups. Then after hydrothermal reduction, the peak at 2θ=10.3°disappeared, and a strong peak at around 24.6° appeared with the interlayer spacing of about 3.6 Å, indicating the reduction of unzipped MWCNTs to CGN. The sawtooth-shaped broad reflection at 42.6° confirmed turbostratic disordered CGN. Compared with the XRD pattern of CGN, the two peaks at 24.6° and 42.6° of CGN were still in the XRD pattern of the CGN/MnO_2 composite, but a new peak at 36.3° appeared, confirming the existence of MnO_2 in the CGN/MnO_2 composite.

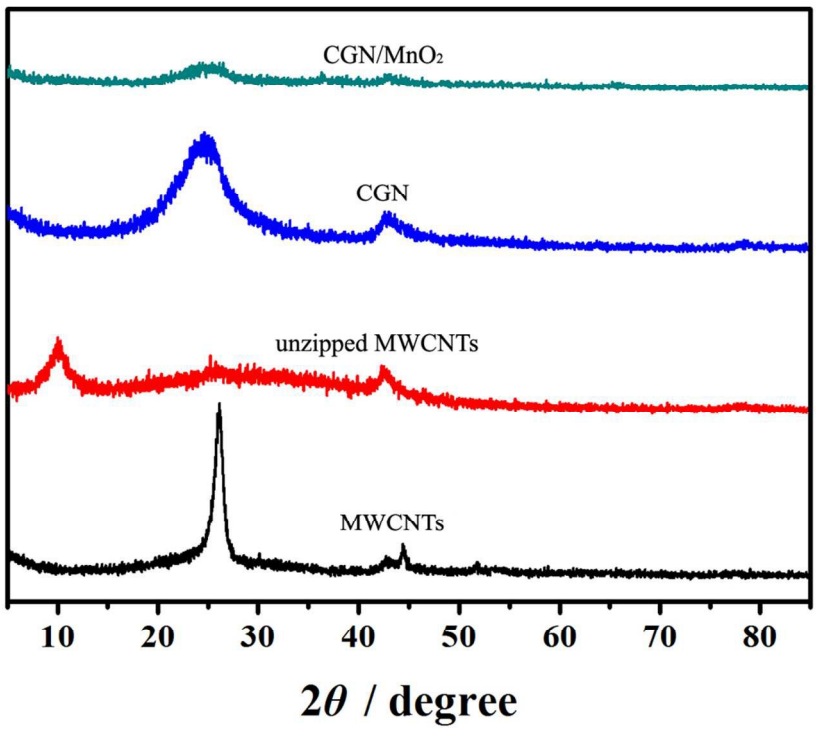

Figure 3 XRD patterns of MWCNTs, unzipped MWCNTs, CGN and CGN/MnO_2.

Raman spectra of CGN/MnO_2 and CGN are displayed in Figure 4, which both exhibited D peak and G peak. A new peak at 644 cm^{-1} appeared in the spectrum of CGN/MnO_2, which was ascribed to the Mn-O vibration. CGN shows a strong D band at 1327 cm^{-1} and a weak G band at 1596 cm^{-1}. After the modification by nanoneedle-like MnO_2, the intensity of D peak and G peak of CGN/MnO_2 declined significantly, while I_D/I_G ratio of CGN (1.43) was almost the same as that of the CGN/MnO_2 (1.44), suggesting the invariable defects.

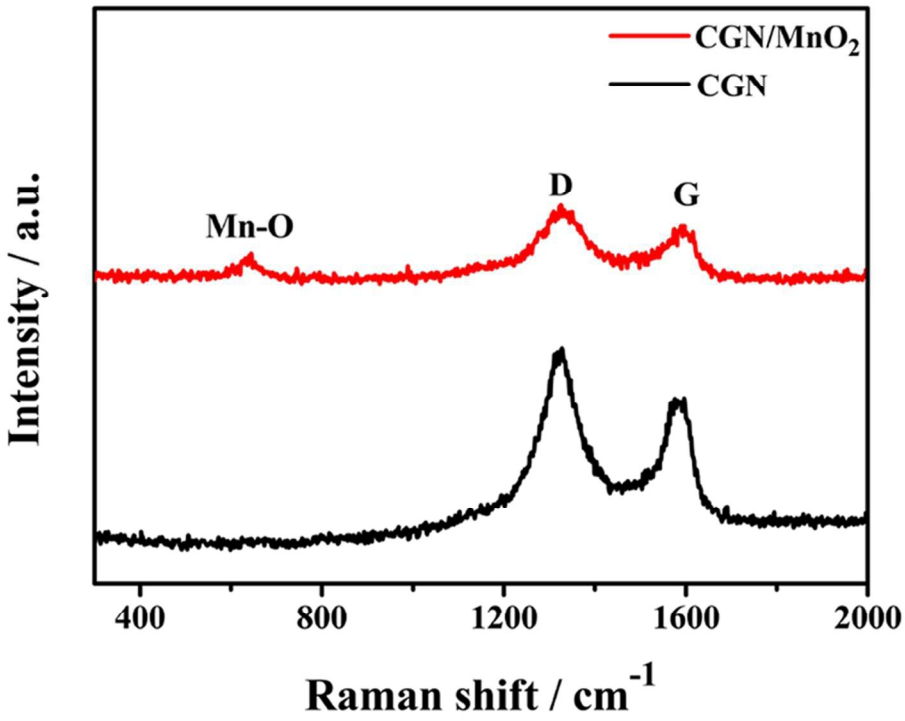

Figure 4 Raman spectra of the CGN and CGN/MnO_2.

Figure 5 shows the N_2 adsorption/desorption isotherms (a) and pore size distribution curves (b) of CGN and CGN/MnO_2. The two N_2 adsorption isotherms displayed type IV with distinct hysteresis loops of type H3 at a relative pressure P/P_0 ranging from 0.45 to 1.00, indicating the existence of mesopores. The specific surface area of CGN/MnO_2 (138 m^2 g^{-1}) is much higher than that of CGN (104 m^2 g^{-1}), indicating nanoneedle-like $MnO_2$was beneficial to the increase of the specific surface area via preventing the restacking and agglomeration of CGN as "spacers". Meanwhile, the increase in specific surface area improved the electric double-layer capacitance of CGN. The pore size distribution was measured using the Barrett-Joyner-Halenda (BJH) method from the desorption branch of the isotherm, which showed a main pore size distribution around 4 nm. The adsorption average pore width of CGN/MnO_2 (10 nm) was obviously smaller than that of CGN (13 nm), and an increase in pore volume was also observed from 0.394 cm^3 g^{-1} for CGN to 0.407 cm^3 g^{-1} for CGN/MnO_2, indicating more pores and bigger specific surface area of CGN/MnO_2. The higher Brunauer-Emmett-Teller (BET) surface area of CGN/MnO_2 contributed to higher specific capacitance of CGN/MnO_2 composite electrode. These results suggest that the control of the mass ratio of CGN to MnO_2 is important to achieve the optimal material utilization.

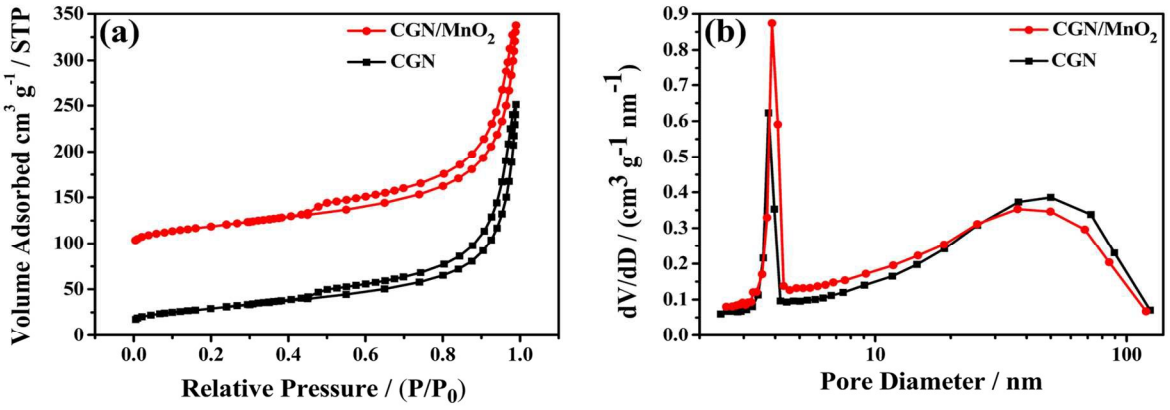

Figure 5(a) Nitrogen adsorption/desorption isotherms and (b) pore size distribution profiles of CGN and CGN/MnO_2.

3.2. Electrochemical performance

The electrochemical impedance spectrum (EIS), cyclic voltammetry (CV), and galvanostatic charge-discharge measurements were performed to test the electrochemical properties of CGN and CGN/MnO_2 composite in 1 M Na_2SO_4 electrolyte. The Nyquist plots shown in Figure 6a displayed similar shape. At the low frequency, the curve of CGN/MnO_2 was more vertical than CGN, indicating better supercapacitive characteristic and larger capacitance of CGN/MnO_2 than CGN. At the high frequency, generally there should appear a semi-circle. Unfortunately, the semi-circle was not clearly observed in this study. The reason might be ascribed to the limitation of the equipment, in which the highest frequency can only go up to 100 kHz. Figure 6b and c show the Bode plots of the CGN and CGN/MnO_2 electrodes.The phase angle and time constant extracted from the Bode plots were 82° and 3 ms for the CGN/MnO_2electrode, and 80° and 5 ms for the CGN electrode. The higher phase angle and lower time constant suggest the better supercapacitive performance of the CGN/MnO_2 electrode.

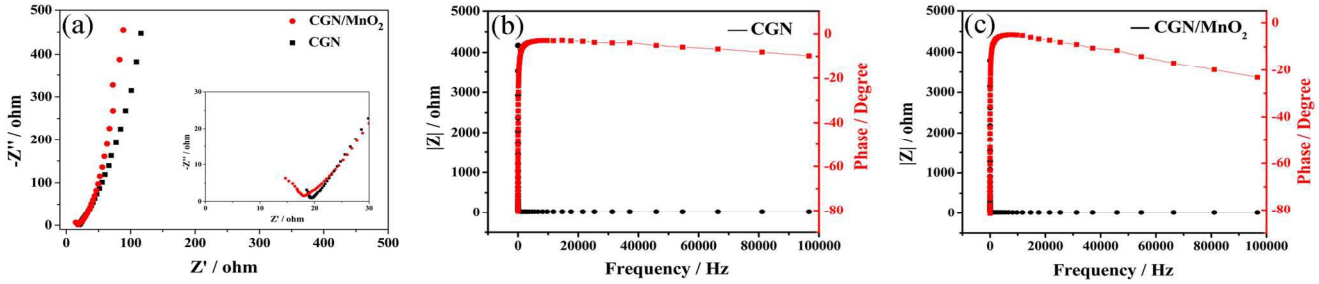

Figure 6(a) Nyquist plots of the CGN and CGN/MnO_2electrodes in 1 M Na_2SO_4, and Bode plots of (b) the CGN and (c) the CGN/MnO_2 electrodes.

Figure 7a shows the CV curves of CGN, MnO_2, and CGN/MnO_2 electrodes at a scan rate of 50 mV s^{-1} in 1 M Na_2SO_4 at the potential range of 0 to 0.8 V. As shown, all the CV curves showed quasi-rectangular shape, displaying their capacitive behavior, but the CGN/MnO_2 composite displayed a superior capacitive behavior with a larger current density than CGN or MnO_2, suggesting a higher specific capacitance of CGN/MnO_2 electrode. Figure 7b shows galvanostatic charge-discharge curves of CGN, MnO_2 and CGN/MnO_2 composite electrodes at a constant current density of 1 A g^{-1} in 1 M Na_2SO_4.The specific capacitance$C$was calculated according to $C = I*\Delta t/(m*\Delta V)$, where C is the specific capacitance in F g^{-1}, I is the constant discharge currentin A, Δt is the discharge timein s, and ΔV is the working voltage in V. As shown, all the charge/discharge curves showed linear line, and the specific capacitances were 73 F g^{-1}, 83 F g^{-1}, and 224 F g^{-1} at 1 A g^{-1} for MnO_2, CGN, and CGN/MnO_2 respectively. The largest specific capacitance of CGN/MnO_2 electrode was contributed by the nanoneedle-like MnO_2, which not only enlarged accessible area of materials to the electrolyte but also reduced the diffusion resistance of ions between them. As the double layer capacitance of CGN was related to the specific surface area of the material, and the specific surface area of CGN/$MnO_2$was 138 m^2 g^{-1}, the interfacial capacitance of CGN in CGN/MnO_2 is 110 F g^{-1}, and the pseudocapacitance reaches 114 F g^{-1}. As the mass ratio of MnO_2 in CGN/MnO_2 is 10 wt%, the pseudocapacitance of MnO_2 is 1140 F g^{-1} when getting rid of the capacitance of CGN. The pseudocapacitance of MnO_2 in CGN/MnO_2 is close to the theoretical specific capacitance value. Meanwhile, as shown in Figure 7a and b, the shapes of both the CV curves and galvanostatic charge-discharge curves of CGN and CGN/MnO_2 composite don't change significantly, which demonstrates the good capacitive performance of nanoneedle-like MnO_2 in the whole charge and discharge potential range. The electronic conductivity of MnO_2 increases because MnO_2 nanoneedles cling to the surface of CGN and the large specific surface area of nanoneedle-like MnO_2 exposed to the electrolyte is beneficial to the full use of its pseudocapacitive performance.

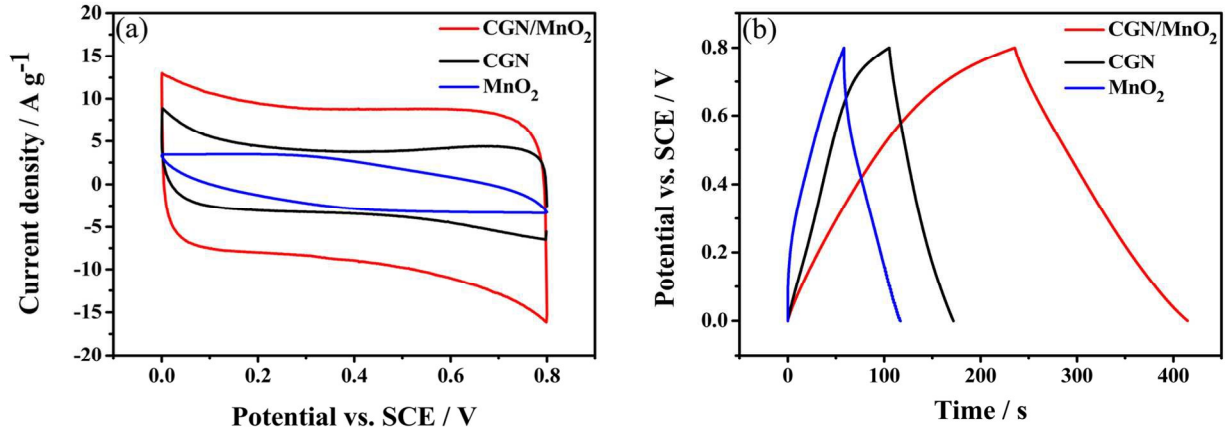

Figure 7(a) CV curves of the CGN, MnO_2, and CGN/MnO_2 electrodes at a scan rate of50 mV s^{-1} in 1 M Na_2SO_4 (b) galvanostatic charge-discharge curves of the CGN, MnO_2, and CGN/MnO_2 electrodes at 1 A g^{-1} in 1 M Na_2SO_4.

Figure 8a shows CV curves of CGN/MnO_2 at different scan rates from 10 to 200 mV s^{-1} in 1 M Na_2SO_4. It can be seen that the CV curves show ideal rectangular shape, demonstrating the excellent capacitive characteristic of the CGN/MnO_2 electrode. Figure 8b shows the charge/discharge curves of the CGN/MnO_2 electrode with symmetrical shape at different current densities. These results verify the very good supercapacitive performance of the CGN/MnO_2 composite electrode.

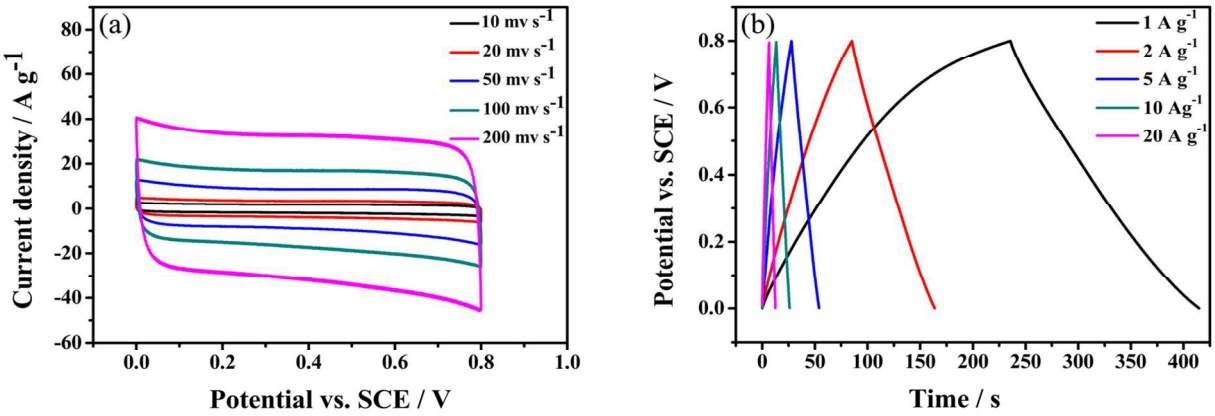

Figure 8(a) CV curves of the CGN/MnO_2 electrode at different scan rates from 10 to 200 mV s^{-1} in 1 M Na_2SO_4 (b) galvanostatic charge/discharge curves of CGN/MnO_2 at different current densities between 1 and 20 A g^{-1} in 1 M Na_2SO_4.

Figure 9 shows the specific capacitance as a function of discharge current densities. The CGN/MnO_2electrode delivered specific capacitances of 224, 196, 164, 158 and 154 F g^{-1} at the current densities of 1, 2, 5, 10 and 20 A g^{-1} respectively. The specific capacitance of CGN/MnO_2composite at 20 A g^{-1} retained 69% of the specific capacitance at 1 A g^{-1}, indicating that the composite exhibited excellent rate capacitive performance. The specific capacitance from 5 A g^{-1} to 20 A g^{-1} almost varies little, indicating high rate charge-rate capability. This is because the electrode has fast electron transfer and ion mobility. The electrical conductivities of the CGN, MnO_2, and CGN/MnO_2 were measured by four-probe conductivity meter. The conductivities of the CGN, MnO_2 and CGN/MnO_2 were 6.8×10^{4} S cm^{-1}, 2.04×10^{-5} S cm^{-1} and 1.35×10^{4} S cm^{-1} respectively. The conductivity study showed that the CGN/MnO_2 composite had a comparative conductivity of the CGN, enabling the fast electron transfer. The tiny MnO_2 and its special nanoneedle-like structure decorated on the CGN facilitated the ion mobility.

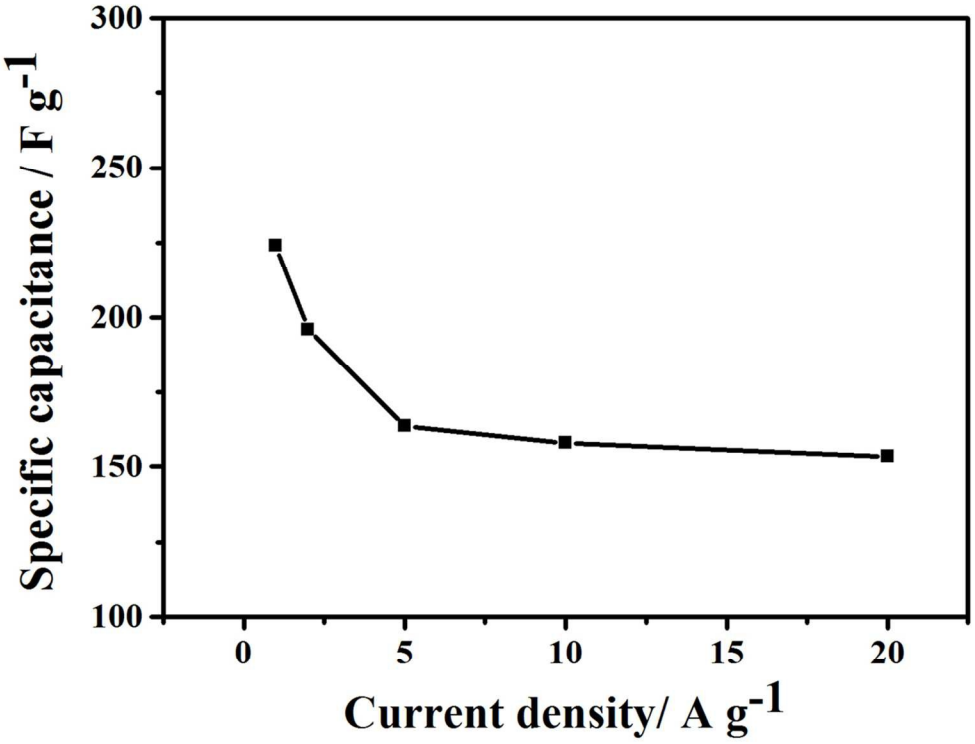

Figure 9 Specific capacitance of CGN/MnO_2 at different current densities from 1 to 20 A g^{-1} in 1 M Na_2SO_4.

To further explore the electrochemical performance of the CGN/MnO_2 composite, a symmetric supercapacitor device was constructed. Figure 10a shows the CV at 50 mV s^{-1} with very good rectangular shape, indicating good supercapacitive characteristic. Figure 10b shows the galvanostatic charge/discharge curves of the symmetric supercapacitor at 1 A g^{-1} with various mass loading. From the discharge curves, the specific capacitances of the supercapacitors were to be 60 F g^{-1}, 49 F g^{-1}, and 48 F g^{-1} at the three different mass loadings, which corresponded to the specific capacitances of 240 F g^{-1}, 196 F g^{-1}, and 192 F g^{-1} respectively of the CGN/MnO_2 composite electrode.

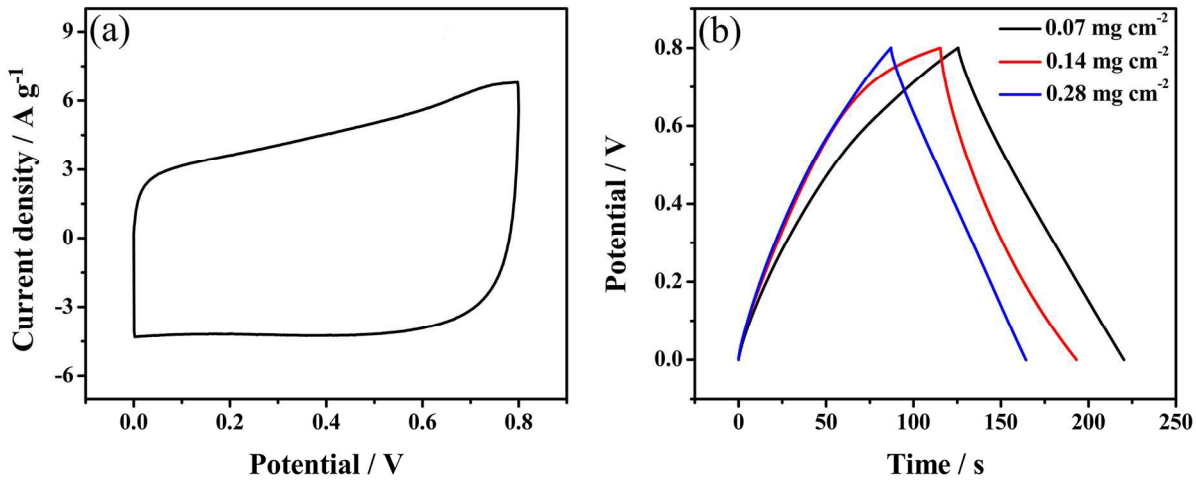

Figure 10(a) CV curve of the CGN/MnO_2 electrode in a two-electrode configuration at a scan rate of 50 mV s^{-1}, and (b) galvanostatic charge/discharge curves of the same two-electrode supercapacitor at 1 A g^{-1} with various mass loading.

A Ragone plot using the data from the two-electrode arrangement is shown in Figure 11, which also contains comparative recent MnO_2-based symmetric and asymmetric supercapacitor data re-plotted from the literature.[42, 43] It's shown that the CGN/MnO_2 composite energy and power density performance was better than others, indicating the good performance of the combination of CGN and MnO_2.

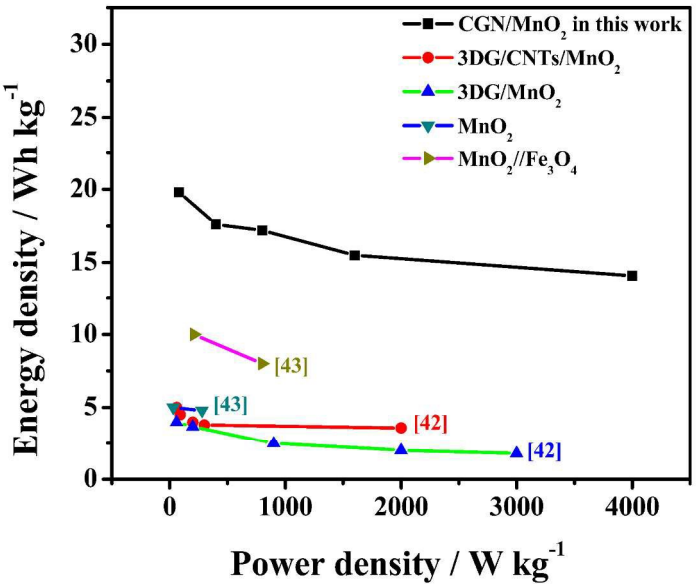

Figure 11 A Ragone plot constructed from data in Figure 10b, together with some comparative re-plotted data of MnO_2-based supercapacitors.

Long term stability up to 10,000 is very helpful to understand the real stability performance.[44, 45] Figure 12 shows the long-term cycling of the CGN/MnO_2 composite, CGN and MnO_2electrodes at 50 mV s^{-1} in 1 M Na_2SO_4. It's interesting that the specific capacitance of CGN/MnO_2 composite electrode increased by 10% of the initial capacitance after 5,000 cycles, and then gradually decreased to 95% of the initial capacitance after 10,000 cycles. The explanation may be that the morphology of the nanoneedle-like MnO_2 slightly changed during cycling, and as a result the specific surface area of CGN/MnO_2 increased leading to the small increase in capacitance. Similar phenomenon was also reported in other studies of MnO_2 electrode.[45] On the contrary, the specific capacitance of the MnO_2 and CGN electrode only retained 12% and 59% respectively. The best cycling performance of CGN/MnO_2 composite electrode was ascribed to the combination of CGN and MnO_2, where MnO_2 was supported by CGN enabling fast electron transfer, and MnO_2 could also prohibit the restacking of CGN.

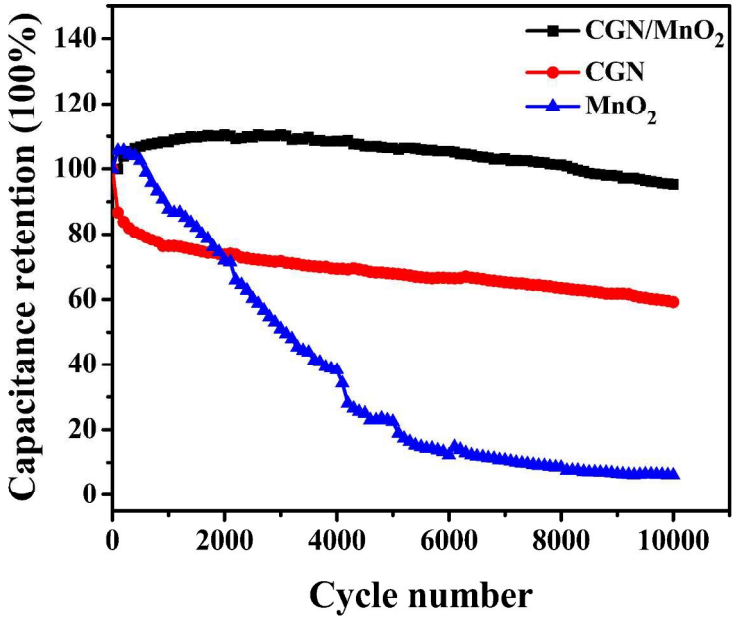

Figure 12 Specific capacitances of the CGN, MnO_2 and CGN/MnO_2 electrodes at 50 mV s^{-1} over 10,000 cycles in 1 M Na_2SO_4.

4. Conclusions

The modified Hummers and hydrothermal methods were employed to synthesize curly grapheme nanosheets, and then MnO_2 nanoneedles were decorated to form a 3D CGN/MnO_2 composite with a CGN to MnO_2 mass ratio of 9:1. In the 3D composite nanomaterials, CGN provided excellent electric double-layer capacitance and was also functioned as a conductive substrate for MnO_2. The uniform distribution of nanoneedle-like MnO_2 with about 5 nm in diameter and about 100 nm in length in CGN was beneficial for the ion diffusion and mass transfer between the electrode materials. As CGN and MnO_2 both performed their own advantages, the performance of CGN/MnO_2 composite was doomed to be the best. This synthetic method of electrochemical supercapacitor composite materials would be a commendable reference for the preparation and application of other composite electrode materials.

Acknowledgements

This work was supported by National Natural Science Foundation of China (Grant No.21271069, J1210040, 51238002, J1103312) and Science and Technology Program of Hunan Province (Grant No.2015JC3049).

Notes and References

1. D. Yu and L. Dai, *The Journal of Physical Chemistry Letters*, 2010, **1**, 467-470.
2. L. Peng, X. Peng, B. Liu, C. Wu, Y. Xie and G. Yu, *Nano Letters*, 2013, **13**, 2151-2157.
3. L. Yuan, X.-H. Lu, X. Xiao, T. Zhai, J. Dai, F. Zhang, B. Hu, X. Wang, L. Gong, J. Chen, C. Hu, Y. Tong, J. Zhou and Z. L. Wang, *ACS Nano*, 2012, **6**, 656-661.
4. Y.-S. Chen and C.-C. Hu, *Electrochemical and Solid-State Letters*, 2003, **6**, A210-A213.
5. G. Hu, C. Tang, C. Li, H. Li, Y. Wang and H. Gong, *Journal of The Electrochemical Society*, 2011, **158**, A695-A699.
6. C. Guan, J. Liu, C. Cheng, H. Li, X. Li, W. Zhou, H. Zhang and H. J. Fan, *Energy & Environmental Science*, 2011, **4**, 4496-4499.
7. Z.-Y. Yang, Y.-F. Zhao, Q.-Q. Xiao, Y.-X. Zhang, L. Jing, Y.-M. Yan and K.-N. Sun, *ACS Applied Materials & Interfaces*, 2014, **6**, 8497-8504.
8. C. Zhang, H. Zhou, X. Yu, D. Shan, T. Ye, Z. Huang and Y. Kuang, *RSC Advances*, 2014, **4**, 11197-11205.
9. J. Wang, Y. Xu, X. Chen and X. Du, *Journal of Power Sources*, 2007, **163**, 1120-1125.
10. W. Yong-gang and Z. Xiao-gang, *Electrochimica Acta*, 2004, **49**, 1957-1962.
11. S. Park and R. S. Ruoff, *Nature nanotechnology*, 2009, **4**, 217-224.
12. E. Frackowiak, *Physical Chemistry Chemical Physics*, 2007, **9**, 1774-1785.
13. S. Frank, P. Poncharal, Z. L. Wang and W. A. d. Heer, *Science*, 1998, **280**, 1744-1746.
14. W. Liang, M. Bockrath, D. Bozovic, J. H. Hafner, M. Tinkham and H. Park, *Nature*, 2001, **411**, 665-669.
15. R. H. Baughman, A. A. Zakhidov and W. A. de Heer, *Science*, 2002, **297**, 787-792.
16. P. Kim, L. Shi, A. Majumdar and P. L. McEuen, *Physical review letters*, 2001, **87**, 215502.
17. M. Kociak, A. Y. Kasumov, S. Guéron, B. Reulet, Khodos, II, Y. B. Gorbatov, V. T. Volkov, L. Vaccarini and H. Bouchiat, *Physical review letters*, 2001, **86**, 2416.
18. Z. K. Tang, L. Zhang, N. Wang, X. X. Zhang, G. H. Wen, G. D. Li, J. N. Wang, C. T. Chan and P. Sheng, *Science*, 2001, **292**, 2462-2465.
19. E. W. Wong, P. E. Sheehan and C. M. Lieber, *Science*, 1997, **277**, 1971-1975.
20. D. A. Walters, L. M. Ericson, M. J. Casavant, J. Liu, D. T. Colbert, K. A. Smith and R. E. Smalley, *Applied Physics Letters*, 1999, **74**, 3803-3805.
21. M.-F. Yu, B. S. Files, S. Arepalli and R. S. Ruoff, *Physical review letters*, 2000, **84**, 5552.
22. K. H. An, W. S. Kim, Y. S. Park, J.-M. Moon, D. J. Bae, S. C. Lim, Y. S. Lee and Y. H. Lee, *Advanced functional materials*, 2001, **11**, 387-392.
23. C.-M. Yang, Y.-J. Kim, M. Endo, H. Kanoh, M. Yudasaka, S. Iijima and K. Kaneko, *Journal of the American Chemical Society*, 2006, **129**, 20-21.
24. E. Frackowiak and F. Béguin, *Carbon*, 2001, **39**, 937-950.
25. D. V. Kosynkin, A. L. Higginbotham, A. Sinitskii, J. R. Lomeda, A. Dimiev, B. K. Price and J. M. Tour, *Nature*, 2009, **458**, 872-876.
26. Y. Wang, Z. Shi and J. Yin, *The Journal of Physical Chemistry C*, 2010, **114**, 19621-19628.
27. R. John, D. B. Shinde, L. Liu, F. Ding, Z. Xu, C. Vijayan, V. K. Pillai and T. Pradeep, *ACS Nano*, 2014, **8**, 234-242.
28. J. M. Miller, B. Dunn, T. D. Tran and R. W. Pekala, *Journal of the Electrochemical Society*, 1997, **144**, L309-L311.
29. C. Yuan, X. Zhang, L. Su, B. Gao and L. Shen, *Journal of Materials Chemistry*, 2009, **19**, 5772-5777.
30. G. Yu, L. Hu, M. Vosgueritchian, H. Wang, X. Xie, J. R. McDonough, X. Cui, Y. Cui and Z. Bao, *Nano letters*, 2011, **11**, 2905-2911.
31. H. Cheng, Z. G. Lu, J. Q. Deng, C. Y. Chung, K. Zhang and Y. Y. Li, *Nano Research*, 2010, **3**, 895-901.
32. C.-C. Hu, K.-H. Chang, M.-C. Lin and Y.-T. Wu, *Nano Letters*, 2006, **6**, 2690-2695.
33. K. Sakiyama, S. Onishi, K. Ishihara, K. Orita, T. Kajiyama, N. Hosoda and T. Hara, *ChemInform*, 1993, **24**, no-no.
34. H. Lee, M. S. Cho, I. H. Kim, J. D. Nam and Y. Lee, *Synthetic Metals*, 2010, **160**, 1055-1059.

35. Q. X. Jia, S. G. Song, X. D. Wu, J. H. Cho, S. R. Foltyn, A. T. Findikoglu and J. L. Smith, *Applied Physics Letters*, 1996, **68**, 1069-1071.
36. W. Wei, X. Cui, W. Chen and D. G. Ivey, *Chemical Society Reviews*, 2011, **40**, 1697-1721.
37. M. Toupin, T. Brousse and D. Bélanger, *Chemistry of Materials*, 2004.
38. D. Bélanger, L. Brousse and J. W. Long, *The Electrochemical Society Interface*, 2008, **17**, 49.
39. E. Raymundo-Piñero, V. Khomenko, E. Frackowiak and F. Béguin, *Journal of The Electrochemical Society*, 2005, **152**, A229-A235.
40. S.-B. Ma, K.-W. Nam, W.-S. Yoon, X.-Q. Yang, K.-Y. Ahn, K.-H. Oh and K.-B. Kim, *Journal of Power Sources*, 2008, **178**, 483-489.
41. S. Chen, J. Zhu, X. Wu, Q. Han and X. Wang, *ACS Nano*, 2010, **4**, 2822-2830.
42. C. Wanjun, H. Yongmin, L. Xiaodong, Z. Jinyuan, Z. Zhenxing, Z. Changhui, G. Chengshi, L. Shuankui, P. Xiaojun and X. Erqing, *Nanoscale*, 2013, **5**, 11733-11741.
43. J. W. Long, D. Bélanger, T. Brousse, W. Sugimoto, M. B. Sassin and O. Crosnier, *MRS Bulletin*, 2011, **36**, 513-522.
44. L. Demarconnay, E. Raymundo-Piñero and F. Béguin, *Journal of Power Sources*, 2011, **196**, 580-586.
45. L. Demarconnay, E. Raymundo-Piñero and F. Béguin, *Electrochemistry Communications*, 2010, **12**, 1275-1278.